Journal of Nano- and Electronic Physics
Vol. **15** No 6, 06027(5pp) (2023)

Журнал нано- та електронної фізики
Том **15** № 6, 06027(5cc) (2023)

Influence of Wafer Thickness and Screen-Printing Mesh Counts on the Al-BSF in Crystalline Silicon Solar Cells

B. Labdelli[1,2,*], A. Djelloul[1,†], L. Benharrat[1], A. Boucheham[1], H. Mazari[2], R. Chalal[1], A. Manseri[1]

[1] *Centre de Recherche en Technologie des Semi-Conducteurs pour l'Energétique 'CRTSE', 02 Bd Frantz Fanon, BP 140, 7 Merveilles, Alger, Algérie*
[2] *Laboratory, Department of Electronics, Sidi Bel Abbes University, B.P. 89, 22000 Algeria*

(Received 15 September 2023; revised manuscript received 14 December 2023; published online 27 December 2023)

In this study, experiments on the alloying process from screen-printed aluminum (Al) pastes on silicon surfaces for solar cell applications were conducted. We investigated the effect of wafer thickness and screen-printing mesh counts on the Al back surface field (Al-BSF) properties of Czochralski silicon (Cz-Si) solar cells Screens with different mesh counts (150, 200 and 400 mesh) were used to print variable amounts of Al paste (7, 9.4 and 12 mg/cm^2). Rapid thermal annealing (RTP) annealing processes of 750 °C and 800 °C for 60 s were applied to form AL-BSF. SEM micrographs showed the formation of a rough surface with 4.31 μm alloying layer over bulk Si wafer. ECV and SIMS analysis showed that an annealing peak temperature of 750 °C and an amount of Al paste of 12 mg/cm^2 are suitable for the creation of an optimal Al-BSF. This work revealed that Al-BSF properties are strongly affected by the mesh counts used in screen-printing of Al paste. However, no monotonic relationship was noticed with the wafer thickness. The mask with 150 meshes allowed to obtain high Al concentrations at the surface, maximum diffusion depth and longer average lifetimes of charge carriers.

Keywords: Rapid Thermal Processing, Screen-printing, Al-BSF, Silicon, Solar Cell.

DOI: 10.21272/jnep.15(6).06027 PACS numbers: 61.72.Cc, 81.15._z, 61.72.uf, 84.60.Jt

1. INTRODUCTION

The back-surface field (BSF) consists of a highly doped area on the back surface of a solar cell which is formed to reduce the effects of rear surface recombination velocity on voltage and current if the rear surface is closer than a diffusion length to the junction [1-8]. Aluminum (Al) is considered the most important acceptor dopants in silicon (Si) and the contact between the high and low doped regions acts like a p-n junction [9]. At the contact, an electric field, introducing a barrier to the flow of minority carrier to the rear surface. As a result, the minority carrier concentration remains higher in the bulk of the device, and the BSF has the net effect of passivating the rear surface [10]. Al-BSF is used in the manufacture of *p*-type silicon solar cells due to its process simplicity and cost-effectiveness. The screen printing of Al paste on the back surface of silicon (Si) at the end of the processing sequence of a solar cell is followed by firing at high temperature to obtain an Al-p^+ doped silicon layer [11-13]. The Al-BSF is one the passivation technique that has a significant impact in improving the performance of the solar cell; it is applied to the back of the cell creating a repulsive field which allows reflecting the minority charge carriers and return them to the junction.

Many experiments have been conducted to investigate Al alloying mechanism for the formation of high quality p^+ regions in solar cells [14-16]. During the screen-printing process, the local contact formation is often realized by printing Al paste on a locally opened dielectric layer [17]. As a result, electrons migrate from the *p* region to fill neighboring holes in the p^+ material, resulting in the creation of a repulsive field that prevents further electron migration. During a rapid thermal process (RTP) [18] which consists in heating the Al layer deposited on the back surface of the solar cell above the eutectic temperature (577 °C), an Al-Si liquidus is created. As the alloying temperature increases, further interdiffusion occurs at the interface between Si and Al forming Al-Si melt which starts to penetrates into the Si bulk. After reaching a maximum temperature for a short time, the wafer is cooled down and the solidification process takes place forming the p^+-doped region (BSF). Thus, the BSF is formed by both, epitaxially recrystallization of Si from the Al-Si melt, which is highly doped by Al atoms, and by incorporation of Al atoms in the Si lattice [19-21].

However, owing to the better effect of the alloying process on Al-BSF formation, it would be interesting to investigate the properties of the formed Al-BSF as a function of the mesh counts of the mask used in screen-printing of Al paste and wafer thickness which both have a direct effect on the cost and performance of solar cells. Along with the thinning crystalline Si (*c*-Si) wafer which avoids the use of expensive and energy-intensive Si material, the required diffusion length of minority carriers is shorter in a thinned Si bulk, allowing the use of wafers with shorter carrier lifetimes [22]. In the present study, the influence of wafer thickness and Al paste amount on the Al-BSF properties in crystalline silicon solar cells was investigated.

2. EXPERIMENTAL DETAILS

2.1 Material and Methods

p-type 100 Cz-Si wafers with a resistivity of 1-3 Ohm·cm were used to evaluate the electrical proper-

*boutaleb200574@yahoo.fr
†djelloulcrtse@gmail.com

ties of the Al-BSF and the passivation efficiency, respectively. First, the thinning of four wafers was performed in NaOH + H_2O, yielding thicknesses of 400, 380, 280, and 220 μm. After chemical cleaning of wafers using Piranha solution (H_2SO_4:H_2O_2), three separate screens with different number of meshes were used to monitor the amount of the printed Al paste. Different mesh counts have been used 400, 200 and 150 Mesh abbreviated BSF1, BSF2 and BSF3, respectively, the wafers were weighted before and after the Al printing to ensure a precise evaluation of the past amount. The commercially available Al paste was screen-printed on the full-area of the wafer surface and dried to remove the solvents. The printed amount of Al paste was found to range from 7, 9.4 to 12 mg/cm². The screen-printing process is followed by an RTP firing at a peak temperature (T_{peak}) of 750 °C and 800 °C in N_2/O_2 mixture environment. The firing process lasts 60 seconds and comprises two ramps, the first from 0 °C to 550 °C taking 10 seconds and the second from 550 °C to the highest temperature taking 20 seconds. A liquid Al-Si alloy is formed at 660 °C. During the cooling-down process, the alloy shrinks and leaves a sheet of p^+ doped silicon behind, allowing the passivation by field effect and reducing recombination on the back side. Hot 37% hydrochloric (HCl) and phosphorus (H_3PO_4) acids were used to remove the remaining Al coating from the surface.

2.2 Characterization

The characterization techniques used were mainly four-point probe (CMT-SR2000N, Chang-Min Co, Ltd., 2000) to measure the resistivity, quasi-steady-state photo-conductance (QSSPC) for life-time measurements, scanning electron microscopy (SEM) and energy dispersive spectrometer (EDS) for morphology and chemical composition analysis, electrochemical capacitance-voltage (ECV) profiler PN 4300-PC and secondary ion mass spectroscopy (SIMS) to perform doping profile measurements.

3. RESULTS AND DISCUSSION

3.1 Morphological Properties (Surface Roughness)

After Al stripping, the topographic quality of the surface obtained is evaluated by measuring the arithmetic mean roughness (R_a) with a TESA-RUGO SCAN roughness meter with a scanning pitch varying between 1 μm and 5 μm. This widely used parameter is defined by the following relation

$$R_a = \frac{1}{n}\sum_{i=L}^{n}|Y_L|. \quad (1)$$

With, Y_L are the distances between the mean line and the profile; n is the number of measured values.

Thus, the degree of roughness depends heavily on the printing and alloying conditions; the less Al paste used, the rougher the surface is expected. In this study, we performed with a series of R_a measurements on two silicon wafers etched with different solutions (HCl and H_3PO_4). The results obtained of roughness are presented in Fig. 1. One may observe that Ra varies between 0.85 μm and 1 μm for a mask of 400 meshes.

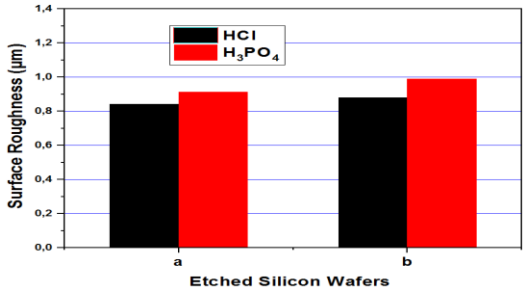

Fig. 1 – Surface roughness (Ra) measured on surfaces of silicon wafers etched with HCl and H_3PO_4 solutions (400 mesh mask)

The obtained Ra measurements reveal that the surface etched using HCl solution is less rough than the surface etched by the H_3PO_4 solution.

For a deeper understanding of the morphology of the surface, roughness measurements were completed by SEM observations. The SEM micrographs (obtained using secondary electrons) of the samples revealed the presence of metallic precipitates at the surface of the wafers (Fig. 2).

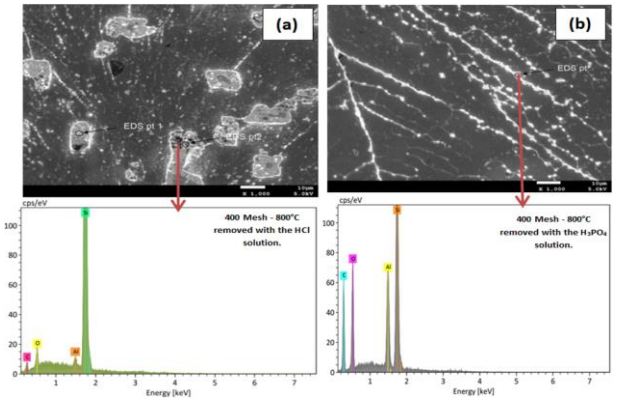

Fig. 2 – SEM micrographs and corresponding EDS analysis of Al-p^+ region after etching the surface in (a) 37 % HCl boiled solution, and (b) in H_3PO_4 solution

EDS analysis of the etched surfaces of wafers by HCL and H_3PO_4 revealed the presence of C, O, Si, and Al, with higher amounts of Al for the wafer etched with H_3PO_4 than for that etched with HCl, indicating that the latter is more effective for Al surface etching. Figure 3 depicts the cross-sectional SEM observations of typical Al-p^+ region.

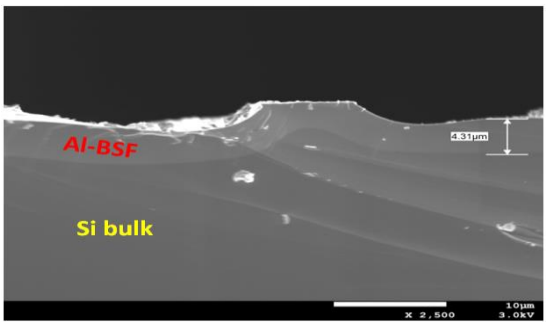

Fig. 3 – Cross-sectional SEM micrograph of a typical Al-p^+ region

The SEM surface analysis after Al etching exhibited a very rough surface at annealing temperatures of 800 °C (Fig. 2). The cross-sectional SEM micrographs

showed a sharp relief of the wafer surface with an Al-BSF region close to 4.3 μm thickness over bulk Si ECV measurements profiles (Fig. 3).

The electrically active doping concentrations are determined using the ECV technique with a diluted ammonium biflouride (NH_4HF_2) electrolyte.

3.2 ECV Measurement Profiles

The electrically active doping concentrations are determined using the ECV technique with a diluted ammonium biflouride (NH_4HF_2) electrolyte.

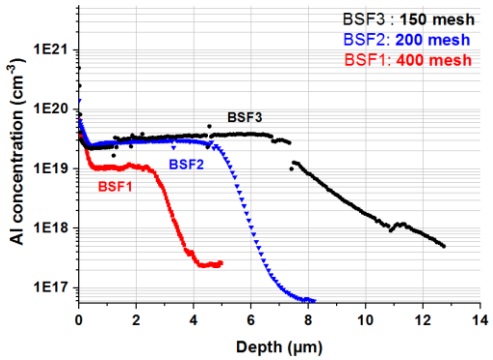

Fig. 4 – ECV profiles for three silicon wafers of the same thickness with different concentrations of Al deposited (400, 200 and 150 meshes)

Different amounts of Al paste were applied to three silicon wafers of the same thickness 7, 9.4 and 12 mg/cm^2, which are represented by BSF1, BSF2, and BSF3, respectively (Table 1). One may observe that the number of meshes and the amount of Al deposited had an inverse relationship. The ECV measurement (Fig. 4) shows clearly that the number of meshes affects the surface concentrations and doping profiles of Al for the same annealing profile. The deposited Al amount increases as the mesh number decreases, which explains why the Al concentration at the surface has increased. The doping depth of Al follows the same trend it can be noticed from Table 1 that the mask with 150 meshes allows to obtain higher Al concentration at the surface as well as a deeper BSF taking into account that the same annealing profile is applied for the three wafers.

Table 1 – Physical properties of BSF as a function of the mesh counts

Samples	Printed amount of Al paste (mg/cm^2)	Al Concentration (At/cm^3)	Depth (μm)
BSF1 (400 mesh)	7	1 E+19	2.5
BSF2 (200 mesh)	9.4	3 E+19	4.5
BSF3 (150 mesh)	12	3.5 E+19	6.5

3.3 Impact of Peak Firing Temperature

Fig. 5 shows the qualitative analysis of doping profiles by SIMS performed at two peak temperatures of 750 °C (a) and 800 °C (b) with different amounts of Al deposited.

SIMS analysis confirmed these findings. With the Al residues left over from the samples' low surface etching in mind, several interpretations were created. After 500 and 400 seconds of pulverization time, respectively, the true profiles for 750 and 800 °C were obtained.

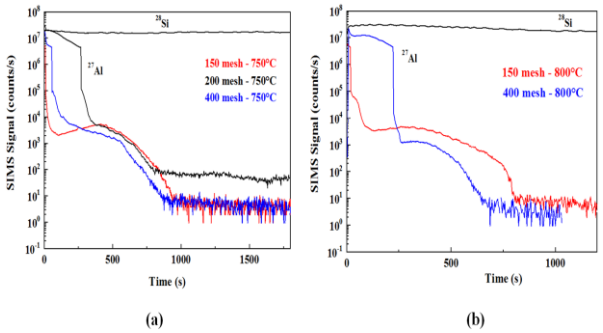

Fig. 5 – SIMS profiles of Al annealed by RTP at (a) 750 °C and (b) 850 °C for different mesh counts

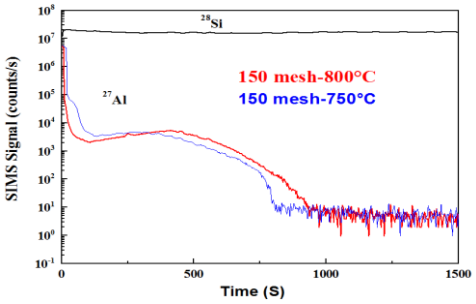

Fig. 6 – Influence of annealing peak temperature on the Al profile

The peak annealing temperature has been adjusted for the same volume of deposited Al to investigate the influence of the peak annealing temperature on the Al alloying profile. Fig. 6 depicts two temperature profiles applied to samples of the same quantity of Al paste (150 mesh: 12 mg/cm^2), demonstrating that the surface concentration as well as the depth of Al penetration increase with the increase of peak RTP annealing temperature.

3.4 Variation of the Sheet Resistance

The changes in sheet resistance and effective lifetime of minority carriers were examined as a function of the number of meshes (mesh counts), wafer thickness, and RTP annealing peak temperature.

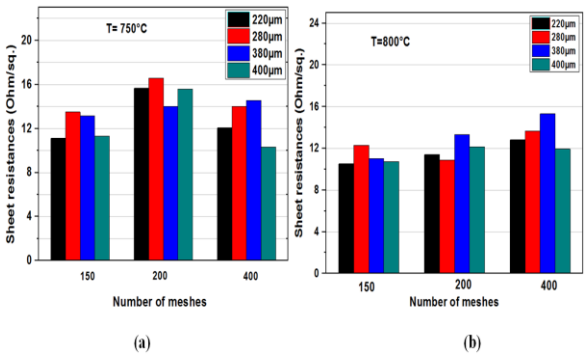

Fig. 7 – Variation of sheet resistance as a function of the number of mesh for different wafer thicknesses and annealing peak temperatures (a) T_{peak} = 750 °C and (b) T_{peak} = 800 °C

The sheet resistances (R_{sh}) are evaluated with the four-point probe measurements as shown in Fig. 7. The overall comparison between graphs (a) and (b) of Fig. 7, indicates that a decrease in sheet resistance with an increase in the annealing peak temperature. One may

suppose that increasing the annealing temperature, leads to further diffusion of Al into Si bulk which enhances the Al concentration in the BSF region.

From Fig. 7, one may also observe that the sheet resistance varies inversely with the number of mesh (mesh counts). A mask with a lower mesh number gives lower sheet resistance due to higher amount of Al deposited as reported in section 3.2 (Table 1). On the other hand, the variation in the thickness of the wafers from 220 µm to 400 µm, does not have a monotonic effect on the sheet resistances of the Al-BSF layer.

3.5 Variation of Effective Lifetime

Fig. 8 represents the findings obtained from QSSPC characterization of symmetrical Al/Si/Al test wafers after RTP annealing and HCl etching at an injection level of $\Delta n = 10^{15}$ cm^3 by varying the peak annealing temperature and the number of mesh in the mask, as well as wafer thickness.

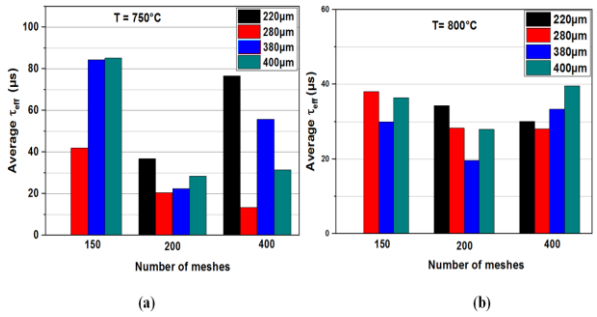

Fig. 8 – Variation of effective lifetime as a function of the number of mesh and wafer thickness annealing peak temperatures (a) T_{peak} = 750 °C and (b) T_{peak} = 800 °C

The BSF obtained with a 150 mesh mask is considered the most efficient. The average effective lifetime obtained is between 40 µs – 85 µs at 750 °C and between 30 µs – 38 µs at 800 °C. This can be explained by the higher concentration of Al on the surface and a deeper diffusion of Al into Si bulk. However, no clear effect on the sheet resistance can be drawn from the variation in wafers thickness, hence, the trend for better passivation or degradation is not visible.

The SH approach uses van der Pauw measurements to determine the conductivity of a wire σs and the Hall coefficient RH. The measurements were taken on a van der Pauw (VDP) structure using the Stripping Hall profiler HL 59 WIN. A Ga/In eutectic alloy is used to produce the ohmic contact.

Fig. 9 depicts the mobility measurements of charge carriers performed on the sample BSF3 for which 12 mg/cm^2 amount of paste was deposited using the 150 mesh mask at two different peak temperatures (750 °C and 800 °C).

The mobility dropped almost to half of its origin value as the peak annealing temperature increased from 750 °C to 800 °C for the same amount of paste deposited. The carrier mobility is sensitive to surface roughness and interface defects [23]; this confirms that the peak temperature of 750 °C allows better passivation which is in accordance with the findings from QSSPC measurements (Fig. 8).

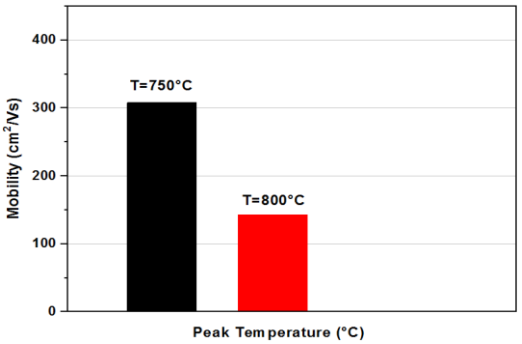

Fig. 9 – Variation of the mobility of charge carriers as a function of peak annealing temperature for a 150 mesh mask

3.6 Variation of Back Surface Reflector (BSR)

Fig. 10 shows the UV-Vis spectra measurements of back-surface reflectance for different samples as a function of (a) mesh number and (b) peak annealing temperature on the range 400 *nm* – 1100 *nm*.

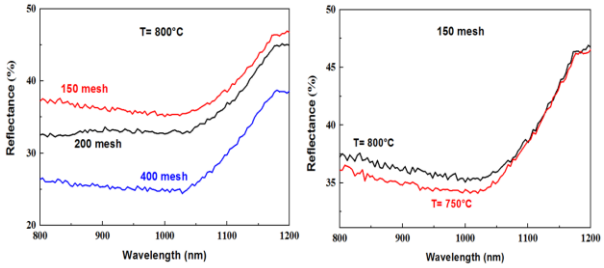

Fig. 10 – Back-reflectance spectra as a function of (a) mesh number and (b) peak annealing temperature

As seen in Fig. 10(a), the average reflectance in the range 800 – 1100 nm decreased as the mesh number increased from 150, 200 to 400. The reflectance varies from 36% for a 150 mesh mask to 25.80% for a 400 mesh mask. However, for a 150 meshes mask (Fig. 8.(b)), the reflectance decreased for the peak annealing temperature 750 °C compared to 800 °C with values dropping from 36 % to 25.27 %, respectively.

4. CONCLUSION

In this study, we investigated the effect of wafer thickness, amount of Al paste and mesh counts of the mask on the Al-BSF properties of Cz-Si solar cells. SEM/EDS observations indicated that H_3PO_4 is more effective for Al surface etching than HCl. The cross-sectional SEM micrograph showed the formation of 4.31 µm alloying layer over bulk Si wafer. According to ECV and SIMS analysis, it was found that an annealing peak temperature of 750 °C and an amount of Al paste of 12 mg/cm^2 are suitable for the creation of an optimal Al-BSF. This work revealed that the properties of Al-BSF are strongly affected by the mesh counts used in the screen-printing of Al paste that there is no monotonic relationship between the thickness of the wafers and the quality of Al-BSF. The best mask for screen-printing Al paste and obtaining good quality Al-BSF was found to be the one with 150 meshes. This mask allowed to obtain high Al concentrations at the

surface, maximum diffusion depth and longer average lifetimes of charge carriers. This work provides a practicable approach for the effective use of Al paste in Al-BSF formation as the alloying process have a direct effect on the cost and performance of Si solar cells.

AKNOWLEDGEMENTS

The authors would like to thank the General Directorate for Scientific Research and Technological Development (DGRST).

REFERENCES

1. F.M. Roberts, E.L.G. Wilkinson, *J. Mater. Sci.* **6**, 189 (1971).
2. R. Bock, J. Schmidt, R. Brendel, H Schuhmann, M. Seibt, *J. Appl. Phys.* **104**, 043701 (2008).
3. M. Rüdiger, M. Rauer, C. Schmiga, M. Hermle, *J. Appl. Phys.* **110**, 024508 (2011).
4. M. Rauer, M. Rüdiger, C. Schmiga, H. Strutzberg, M. Bähr, M. Hermle, S.W. Glunz, *J. Appl. Phys.* **114**, 203702 (2013).
5. M. Rauer, C. Schmiga, M. Glatthaar, S.W. Glunz, *Sol. Energy Mater. Sol. C.* **176**, 295 (2018).
6. T. Yoshikawaz, K. Morita, *J. Electrochem. Soc.* **150** No 8, G465 (2003).
7. V.A. Popovich, M.P.F.H.L. van Maris, M. Janssen, I.J. Bennett, I.M. Richardson, *Mater. Sci. Appl.* **4**, 118 (2013).
8. J. Krause, R. Woehl, M. Rauer, C. Schmiga, J. Wilde, D. Biro, *Sol. Energy Mater. Sol. C.* **95**, 2151 (2011).
9. O. Krause, H. Ryssel, *J. Appl. Phys.* **91**, 9 (2002).
10. A. El Amrani, A. Boucheham, A. Guendouzi, B. Labdelli , C. Nasraoui, R. Si-Kaddour, *Silicon* **14**, 223 (2022).
11. P. Lölgen, Ph.D. Thesis, University of Utrecht, Utrecht, The Netherlands (1995).
12. S. Narasimha, A. Rohatgi, A.W. Weeber, *IEEE Trans. Electron Dev.* **46**, 7 (1999).
13. J.B. Gunn, *J. Electron. Control* **4**, 1 (1958).
14. M. Rauer, C. Schmiga, J. Krause, R. Woehl, M. Hermle, S.W. Glunz, *Energy Procedia* **8**, 200 (2011).
15. V. Meemongkolkiat, K. Nakayashiki, D.S. Kim, R. Kopecek, A. Rohatgi, *J. Electrochem. Soc.* **153** No 1, G53 (2006).
16. Y. Wei, X. Jiang, Y. Lin, X. Yang, G. Li, X. Liu, P. Li, A. Liu, *RSC Adv.* **9**, 6681 (2019).
17. https://www.engineeringtoolbox.com/thermal-expansion-metals-d_859.html
18. J. Horzel, C. Allebe, J. Szlufcik, S. Sivoththaman, *Sol. Energy Mater. Sol. C.* **72**, 263 (2002).
19. J.L. Murray, A.J. McAlister, *Bull. Alloy Phase Diagrams* **5**, 74 (1984).
20. Y. Schiele, F. Book, S. Seren, G. Hahn, B. Terheiden, *Energy Procedia* **27**, 460 (2012).
21. F. Huster, G. Schubert, *Proc. 20th EPVSEC*, 1462 (Barcelona, Spain: 2005).
22. R.A. Sinton and A. Cuevas, *16th European Photovoltaic Solar Energy Conference*, 1152 (1-5 May: Glasgow, UK: 2000).
23. L.J.V.D. Pauw, *Semiconductor Devices: Pioneering Papers*, 174 (1991).

Вплив товщини пластини та кількості сіток трафаретного друку на Al-BSF у кристалічних кремнієвих сонячних елементах

B. Labdelli[1,2], A. Djelloul[1], L. Benharrat[1], A. Boucheham[1], H. Mazari[2], R. Chalal[1], A. Manseri[1]

[1] *Centre de Recherche en Technologie des Semi-Conducteurs pour l'Energétique 'CRTSE', 02 Bd Frantz Fanon, BP 140, 7 Merveilles, Alger, Algérie*

[2] *Laboratory, Department of Electronics, Sidi Bel Abbes University, B.P. 89, 22000 Algeria*

У роботі були проведені експериментальні дослідження процесу легування алюмінієвих (Al) паст, надрукованих трафаретним друком на кремнієвих поверхнях для сонячних елементів. Досліджений вплив товщини пластини та кількості сіток трафаретного друку на властивості поля задньої поверхні Al (Al-BSF) кремнієвих сонячних елементів Чохральського (Cz-Si). Використовувалися екрани з різною кількістю сіток (150, 200 і 400 меш) для друку різної кількості пасти Al (7, 9,4 та 12 мг/см^2). Швидкий термічний відпал (RTP) при 750 °C і 800 °C протягом 60 с був застосований для формування AL-BSF. SEM показав утворення шорсткої поверхні з шаром легуючого шару товщиною 4,31 мкм на об'ємній кремнієвій пластині. Аналіз ECV та SIMS показав, що пікова температура відпалу 750 °C і кількість пасти Al 12 мг/см^2 підходять для створення оптимального Al-BSF. Ця робота виявила, що на властивості Al-BSF сильно впливає кількість меш, яка використовується для трафаретного друку пасти Al. Однак не було помічено монотонного зв'язку з товщиною пластини. Маска з 150 меш дозволила отримати високі концентрації Al на поверхні, максимальну глибину дифузії та більший середній час життя носіїв заряду.

Ключові слова: Швидка термічна обробка, Трафаретний друк, Al-BSF, Кремній, Сонячні батареї.